Why the local-mean-energy approximation should be used in hydrodynamic plasma descriptions instead of the local-field approximation

G. K. Grubert, M. M. Becker, and D. Loffhagen
INP Greifswald, Felix-Hausdorff-Str. 2, 17489 Greifswald, Germany
(Received 11 March 2009; revised manuscript received 15 July 2009; published 22 September 2009)

The local-mean-energy approximation (LMEA) and the local-field approximation (LFA) are commonly applied to include the electron properties like transport and rate coefficients into a hydrodynamic description of gas discharge plasmas. Both the approaches base on the solution of the stationary spatially homogeneous Boltzmann equation for the electron component, but the consequences of these approaches differ drastically. These consequences of using both the approaches are studied and discussed on a kinetic level and by comparison of results of hydrodynamic investigations of low-pressure glow discharge plasmas. It is found that the LMEA is to be strongly recommended for the application to a hydrodynamic description of dc as well as rf discharge plasmas, while the LFA is conditionally suitable to describe dc glow discharges with rough reaction kinetics only and its application to rf discharge plasmas is inappropriate.

DOI: 10.1103/PhysRevE.80.036405 PACS number(s): 51.50.+v, 52.80.−s, 52.25.Dg

I. INTRODUCTION

An adequate theoretical description of gas discharge plasmas requires a sufficiently good characterization of the electron subsystem because it determines decisively the characteristics of the whole plasma. The best way for the electron description consists of their kinetic treatment, where the electron Boltzmann equation is solved. On the one hand, expansion techniques are used for the solution [1–6]. On the other hand, Monte Carlo simulations are applied [7–11]. Additionally, particle-in cell Monte Carlo collision (PIC-MCC) simulations [12–16] or hybrid methods [17–24] can be used to describe all relevant species in the discharge plasma. The latter use a kinetic treatment of the electrons and combine it with a hydrodynamic description of the species considered.

The methods mentioned above are numerically expensive. Therefore, hydrodynamic approaches [25–42] are frequently used to describe gas discharge plasmas. An overview of methods for the theoretical description of low-pressure gas discharges is given in Ref. [43]. Different approximations for the electron properties, i.e., for the rate coefficients of electron collision processes and their transport coefficients, have been developed. In particular, the local-mean-energy approximation (LMEA) [30,32,35,42] and the local-field approximation (LFA) [25,28,38,39] are usually utilized to incorporate the electron transport and rate coefficients into the hydrodynamic description. These approaches base on the solution of the stationary spatially homogeneous electron Boltzmann equation as performed in a wide range of the literature, e.g., in Refs. [1,44–47].

In the present paper, the effects of using the LMEA and the LFA are analyzed. The studies cover the electron kinetic level by comparing LMEA and LFA results with the solution of the inhomogeneous kinetic equation of the electrons as well as the application of these approaches to a hydrodynamic description of dc and rf low-pressure glow discharges. In particular, general features of these approaches are studied and their direct consequences to the global discharge behavior are discussed. The studies have been performed for argon and oxygen plasmas, as typical representatives of noble and reactive gases.

II. KINETIC TREATMENT OF THE ELECTRONS

For the analysis of the electron kinetic behavior, the Boltzmann equation

$$\left(\partial_t + \frac{\mathbf{p}}{m_e}\cdot\nabla_{\mathbf{r}} + \mathbf{F}^{\mathrm{ext}}\cdot\nabla_{\mathbf{p}}\right)\tilde{f}(\mathbf{r},\mathbf{p},t) = \sum_a \left[\mathbb{I}_a^{\mathrm{el}}(\tilde{f}) + \sum_i \mathbb{I}_{i,a}^{\mathrm{in}}(\tilde{f})\right] \tag{1}$$

for the electron momentum distribution function (EMDF) $\tilde{f}(\mathbf{r},\mathbf{p},t)$ depending on the coordinate $\mathbf{r}$, the momentum $\mathbf{p}$, and the time t has to be solved. The electron mass and the corresponding collision integrals of elastic (el) collisions and of the ith inelastic (in) collision process of species a are denoted by m_e, $\mathbb{I}_a^{\mathrm{el}}$, and $\mathbb{I}_{i,a}^{\mathrm{in}}$, respectively.

In the following, a spatially one-dimensional analysis along the axial direction of a discharge arrangement with plane electrodes is performed assuming rotational symmetry. The plane-parallel geometry is shown in Fig. 1. The external force taking effect on the plasma corresponds to the electric field force $F_z^{\mathrm{ext}}(z,t) = -e_0 E(z,t)$ in direction of the rotational axis with the charge of the electrons $-e_0$ and the electric field $E(z,t)$. The latter is determined according to $E(z,t) = -\partial_z \varphi(z,t)$ with the scalar electric potential $\varphi(z,t)$.

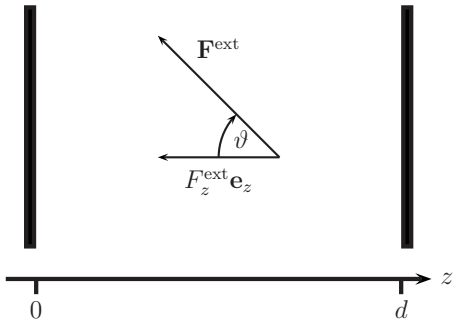

FIG. 1. Axially inhomogeneous discharge geometry between plane electrodes.

Because the plasma inhomogeneity occurs in the direction of the electric field, i.e., parallel to the z direction, an expansion of the EMDF into Legendre polynomials can be performed. This allows a representation of the EMDF by means of expansion coefficients $f_n(z,U,t)$ with $n=0,1,\ldots$ and the electron kinetic energy $U=p^2/(2m_e)$, which can directly be used to determine the macroscopic properties of the electrons. Further information about the resulting set of partial differential equations for f_n and its solution is given in Appendix A.

A. Macroscopic properties

Almost all electron properties of interest are given by appropriate integration of the lowest three expansion coefficients $f_n(z,U,t)$, $n=0,1,2$ over the energy space [4]. For instance, the electron density $n_e(z,t)$ and electron mean energy $\langle U\rangle(z,t)$ have the representation

$$n_e(z,t) = \int_0^\infty dU\sqrt{U} f_0(z,U,t), \tag{2}$$

$$\langle U\rangle(z,t) = \frac{1}{n_e(z,t)} \int_0^\infty dU U^{3/2} f_0(z,U,t), \tag{3}$$

and the rate coefficient $k_i(z,t)$ of the ith inelastic collision process of electrons with the species a is given by

$$k_i(z,t) = \frac{1}{n_e(z,t)} \sqrt{\frac{2}{m_e}} \int_0^\infty dU U f_0(z,U,t) Q_{i,a}^{\mathrm{in}}(U) \tag{4}$$

with the collision cross section $Q_{i,a}^{\mathrm{in}}$ for the process considered with the energy loss or gain $U_{i,a}^{\mathrm{in}}$.

Expressions for the mobility b_e and diffusion coefficient D_e of the electrons are obtained by the combination of the particle flux $\mathbf{j}(z,t)=j_e(z,t)\mathbf{e}_z$ with

$$j_e(z,t) = \frac{1}{3} \sqrt{\frac{2}{m_e}} \int_0^\infty dU U f_1(z,U,t) \tag{5}$$

and the hierarchy equation for $n=1$ [4,48]. The transport properties can be separated according to

$$b_e(z,t) = b_e^0(z,t) + b_e^c(z,t), \tag{6a}$$

$$D_e(z,t) = D_e^0(z,t) + D_e^c(z,t) \tag{6b}$$

into the contributions [48]

$$b_e^0(z,t) = -\frac{1}{3} \sqrt{\frac{2}{m_e}} \frac{e_0}{n_e(z,t)} \int_0^\infty dU \lambda_M(z,U,t) U \partial_U f_0(z,U,t), \tag{7a}$$

$$D_e^0(z,t) = \frac{1}{3} \sqrt{\frac{2}{m_e}} \frac{1}{n_e(z,t)} \int_0^\infty dU \lambda_M(z,U,t) U f_0(z,U,t), \tag{7b}$$

resulting from the commonly used two-term approximation and the additional terms

$$b_e^c(z,t) = -\frac{1}{15} \sqrt{\frac{2}{m_e}} \frac{e_0}{n_e(z,t)} \int_0^\infty dU [2\lambda_M(z,U,t) U \partial_U f_2(z,U,t) + 3\lambda_M(z,U,t) f_2(z,U,t)], \tag{8a}$$

$$D_e^c(z) = \frac{2}{15} \sqrt{\frac{2}{m_e}} \frac{1}{n_e(z,t)} \int_0^\infty dU \lambda_M(z,U,t) U f_2(z,U,t), \tag{8b}$$

resulting from a strict multiterm treatment of the expansion (A1) given in Appendix A. Here

$$\lambda_M(z,U,t) = \left\{ \sum_a n_a(z,t) \left[Q_a^{\mathrm{mt}}(U) + \sum_i Q_{i,a}^{\mathrm{in}}(U) \right] \right\}^{-1}$$

denotes the mean-free path of the electrons with the cross sections Q_a^{mt} for momentum transfer in elastic collisions with the species a having the particle density n_a.

The energy dissipation length

$$\lambda_E(z,U,t) = \lambda_M(z,U,t) \sqrt{\frac{\nu_M(z,U,t)}{3\nu_E(z,U,t)}}$$

can be expressed by the momentum and energy dissipation frequencies ν_M and ν_E, respectively [49]. These frequencies can be obtained from the electron power and momentum balance equations and they read [49]

$$\nu_E(z,U,t) = \sqrt{\frac{2U}{m_e}} \sum_a \left[2\frac{m_e}{m_a} n_a(z,t) Q_a^{\mathrm{mt}}(U) + \sum_{\mathrm{ex,di,io}} n_a(z,t) Q_{i,a}(U) \frac{U_{i,a}}{U} + \sum_{\mathrm{at}} n_a(z,t) Q_{i,a}(U) \right],$$

$$\nu_M(z,U,t) = \sqrt{\frac{2U}{m_e}} \sum_a \sum_i n_a(z,t) Q_{i,a}(U).$$

The corresponding relations for the mobility $\tilde{b}_e$ and diffusion coefficient $\tilde{D}_e$ for the electron energy transport are obtained in an analogous manner by combining the energy flux $\mathbf{\Gamma}(z,t)=\Gamma_e(z,t)\mathbf{e}_z$ with

$$\Gamma_e(z,t) = \frac{1}{3} \sqrt{\frac{2}{m_e}} \int_0^\infty dU U^2 f_1(z,U,t) \tag{9}$$

with the hierarchy equation for $n=1$. They result from the corresponding relations (5), where λ_M in the integral expressions of Eqs. (7) and (8) has to be replaced by $U\lambda_M$.

B. Approximations of the electron properties for hydrodynamic descriptions

Instead of the electron properties resulting from the solution of the space-dependent kinetic description presented in Sec. II A, approaches like the LFA and the LMEA are commonly used. These methods make the properties of the electron component available for hydrodynamic descriptions on the base of solving the stationary spatially homogeneous Boltzmann equation of the electrons [1,44–47]. Here, a modified version of the method presented in Ref. [45] and

adapted to take nonconservative electron collision processes into account [46] has been used. Hence, all electron properties depend on the reduced electric field E/N, where $N=\Sigma_a n_a$ denotes the total gas density. Therefore, the kinetic equation is solved for various E/N resulting in electron properties as functions $g(E/N)$. This is also the reason why this approach is named local-field approximation.

The LFA is very easy to handle in hydrodynamic investigations because the electric field required to obtain the electron properties is determined from the solution of Poisson's equation anyway. As a consequence, there is a direct field dependence of the electron properties. It is well known that the validity of this approach is limited by [50]

$$\frac{1}{\lambda_{E,M}(z,U,t)} \gg \frac{1}{E(z,t)}\partial_z E(z,t), \tag{10a}$$

$$\nu_{E,M}(z,U,t) \gg \frac{1}{E(z,t)}\partial_t E(z,t). \tag{10b}$$

Already in 1946, Morton [51] indicated that the LFA can lead to drastic errors in plasma regions with nonuniform electric fields. Nevertheless, it was used for many investigations because of the reduced numerical effort, e.g., in Refs. [25,28,38,39].

The consideration of the electron energy transport leads to a significant improvement of the description of the electron properties. This ansatz uses the electron mean energy to parametrize the electron transport. That means the required electron quantities are available as functions of the mean energy $\langle U\rangle$ and during the calculation spatial profiles of $\langle U\rangle$ are determined and can be used for the approximation of the electron properties. In the beginning, a Maxwellian electron energy distribution was assumed, which allows the energy-dependent calculation of electron-impact rate coefficients with the corresponding cross-section data [26]. In many cases, the production rates have been represented by Arrhenius' formula as in Refs. [27,29,31]. Later on, the nonequilibrium energy distribution function of the electrons was determined by solving the Boltzmann equation (1) for homogeneous, steady-state plasmas as mentioned above. That means the kinetic equation of the electrons is again solved for different E/N, e.g., in Ref. [30]. However, the resulting macroscopic properties of the electrons are tabulated as functions of the corresponding mean electron energy instead of the reduced electric field. Therefore, the hydrodynamic description involving the LMEA requires the determination of the mean electron energy by considering the electron energy balance equation. In particular, this ansatz has been used for the determination of the ionization rate coefficients only and the electron mobility as well as their diffusion coefficient are used as constants, e.g., in Ref. [32]. This idea has been generalized to all electron-impact collision processes as well as the electron-transport properties [35,42].

The transport and rate coefficients of the electrons for argon and oxygen as functions of E/N and $\langle U\rangle$, respectively, used in the present comparative studies are detailed in Appendix B.

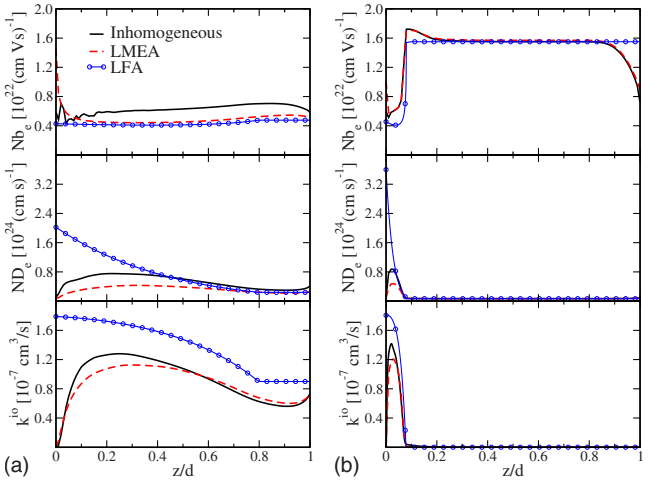

FIG. 2. (Color online) Spatial variation of the mobility b_e, diffusion coefficient D_e, and ionization rate coefficient k^{io} of the electrons obtained by spatially inhomogeneous Boltzmann calculations, LMEA, and LFA in dc oxygen discharges at an applied voltage of −500 V and at pressures of (a) $p=10$ and (b) 100 Pa, respectively.

C. Comparison of the electron properties

Results for the mobility, the diffusion, and ionization rate coefficients of the electrons for abnormal dc oxygen glow discharges at steady state obtained by the strict kinetic treatment as well as by the LMEA and LFA are shown in Fig. 2. The two pressures of 10 and 100 Pa and a cathode-fall voltage of −500 V have been taken for the studies. The electrode gap has been chosen to be $d=2.5$ cm. Due to the fact that pure kinetic calculations cannot determine the space-charge field in the discharge volume, a potential course was set with respect to the similarity properties of abnormal oxygen glow discharges according to Ref. [52]. In particular, a quadratically decreasing function in the cathode-fall region and a linearly decreasing course elsewhere were employed for the magnitude of the electric potential [53].

In order to compare the macroscopic properties of the electrons obtained by the solution of the spatially inhomogeneous electron Boltzmann equation using the multiterm method detailed in Ref. [53] with those determined by the LMEA, the spatial profile of the mean electron energy resulting from the strict kinetic calculation was used. The corresponding LFA results base on the given electric field profile and represent the electron properties as function of the respective profile of E/N in agreement with Fig. 10(c) in Appendix B.

The general spatial behavior of the rate and transport coefficients is comparable for both the pressures. At the higher pressure of 100 Pa [Fig. 2(b)], a fast spatial relaxation to constant values of the electron properties can be seen for all approaches considered. At a distance of $z/d>0.2$, a region is formed where all approximations result in the same values of the electron quantities. In contrast to that, at the lower pressure of 10 Pa [Fig. 2(a)] such strong spatial relaxation cannot be observed due to the smaller collision probability. Therefore, spatial deviations of the LMEA and LFA from the strict inhomogeneous solution occur in the whole discharge region.

Obviously, the LFA should not be used for too small discharges pressures because this approximation results in too high values of the transport properties and rate coefficients for the high-field situation in front of the cathode where condition (10a) is violated. In contrast to the LFA, the LMEA reproduces the spatial profile of the strict solution with slight deviations in the absolute values.

The LFA does not provide physically reasonable results in front of the electrodes. When approaching the cathode, a decrease in the diffusion and ionization rate coefficient is expected, but the LFA strongly overestimates both the quantities close to the cathode because of the increasing electric field action. Such behavior is expected due to the violation of condition (10a). This overestimation of these electron properties can be avoided if the electron energy transport is taken into account by the LMEA. This approach predicts qualitatively the same profiles of the considered quantities as the strict inhomogeneous solution with quantitatively small deviations. In addition, the behavior in front of the anode differs appreciably. The strict solution as well as the LMEA lead to an increase in the diffusion coefficient for both the pressures caused by the depopulation of slow electrons due to their absorption at this electrode [54]. The LFA cannot reproduce this behavior because the major dependence is the underlying electric field. The resulting diffusion-driven flux has to be compensated by a field-driven flux to conserve the space-independent total electron flux in front of the anode, too. The expected decrease in the electron mobility is found for both the pressures using the LMEA and the strict solution, but it is not obtained when applying the LFA although condition (10a) is fulfilled.

The results of the electron kinetic calculations indicate that the LFA can lead to unphysical predictions of discharge plasmas although its validity condition is fulfilled and that the LMEA should be used instead in the framework of a hydrodynamic description. The results in this section have been presented for oxygen discharges. Considering abnormal glow discharges in argon, comparable results have been obtained. In the next section, the influence of both these approaches using a macroscopic description for all species in the considered discharge is discussed.

III. APPLICATION OF THE LMEA AND LFA TO HYDRODYNAMIC DESCRIPTIONS

In the previous section, the strong influence of the various approximations on the rate and transport coefficients of the electrons has been illustrated. Now, the LMEA and the LFA, respectively, are included into a hydrodynamic description of the discharge plasma to treat the behavior of the electrons. The corresponding fluid approach consists of the particle balance equation for each species, the electron energy balance when using the LMEA, and the Poisson equation for the self-consistent determination of the electric potential. These basic equations have the representation

$$\partial_t n_a(z,t) + \partial_z j_a(z,t) = \sum_i \bar{k}_{i,a}(z,t) \prod_{b \in B(i)} n_b(z,t), \quad (11a)$$

$$\partial_t \tilde{U}(z,t) + \partial_z \Gamma_e(z,t) = -e_0 E(z,t) j_e - n_e \mathbb{P}(z,t), \quad (11b)$$

$$\partial_z^2 \varphi(z,t) = -\frac{e_0}{\varepsilon_0} \sum_a Z_a n_a(z,t), \quad (11c)$$

where $B(i)$ denotes the set of species indices corresponding to reaction i. The quantity $\bar{k}_i$ for the reaction i of the species a with the charge number Z_a is defined by $\bar{k}_{i,a}=k_i g_{i,a}$, where $g_{i,a} \in \mathbb{Z}\backslash\{0\}$ determines the number of particles of the species a that are generated or destroyed in the reaction i with the rate coefficient k_i. Here, $\tilde{U}$ denotes the electron energy density and the quantity $\mathbb{P}$ describes the individual contributions of elastic and different kinds of inelastic collisions of electrons with other species to the energy dissipation as detailed, e.g., in Ref. [55]. The particle and energy fluxes in z direction are described by the drift-diffusion approximation

$$j_a(z,t) = Z_a b_a(z,t) n_a(z,t) E(z,t) - \partial_z [D_a(z,t) n_a(z,t)], \quad (12a)$$

$$\Gamma_e(z,t) = -\tilde{b}_e(z,t) n_e(z,t) E(z,t) - \partial_z [\tilde{D}_e(z,t) n_e(z,t)], \quad (12b)$$

where the mobility is represented according to $b_a=e_0/(\mu_{ab}\nu_{ab})$ with the reduced mass μ_{ab} and the transport frequency ν_{ab} of collisions [56]. For the numerical solution of the set of coupled partial differential equations (11) involving Eqs. (12), a finite-element method has been adapted. Because significant contributions of the first spatial derivatives (drift terms) can occur in the continuity equations of the charged particles and the electron energy equation [57], an upwind Petrov-Galerkin finite-element method has been used to achieve a stabilized spatial discretization of these equations. Furthermore, the continuity equation of the neutral particles and Poisson's equation have been discretized by means of the standard Galerkin finite-element method. An implicit time-step method has been used for the determination of the particle densities, and the mean electron energy and the solution of the space-charge field is obtained by applying a semi-implicit potential treatment [58].

The boundary conditions for Eqs. (11a) and (11b) have been chosen in accordance with Hagelaar *et al.* [59]. The conditions for the particle and energy fluxes at the electrodes include particle reflection and secondary-electron emission. Additionally, a distinction between plasma and reflected electrons has been taken into account. The electrode at $z=0$ in Fig. 1 is powered and the electrode at $z=d$ is grounded during the calculations. Details of the solution method are reported in Ref. [57].

In the following, results of hydrodynamic calculations using the electron properties in LMEA and LFA, respectively, are presented for various discharge conditions. In the framework of hydrodynamic modeling using the LMEA, the transport properties and rate coefficients of the electrons are employed as functions of $\langle U\rangle(z,t)$. This mean electron energy $\langle U\rangle=\tilde{U}/n_e$ is obtained from the electron particle density n_e and energy density $\tilde{U}$ determined by Eqs. (11a) and (11b).

The application of E/N-dependent electron-transport coefficients in hydrodynamic descriptions using the LFA results in numerical instabilities and a numerical solution is possible

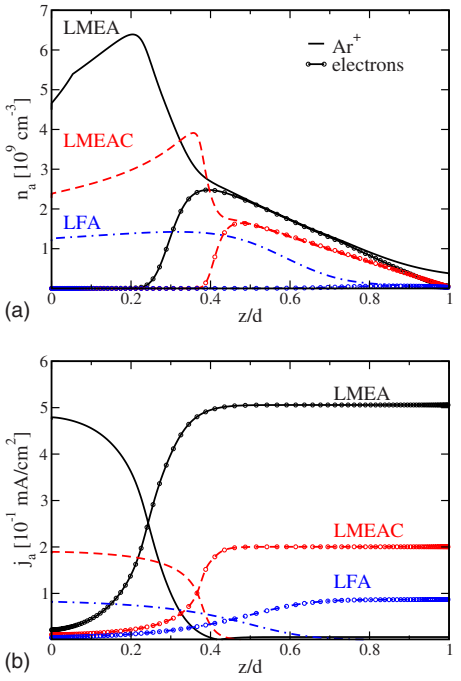

FIG. 3. (Color online) (a) Particle and (b) current densities of electrons and Ar^+ ions as a function of the space coordinate z obtained by hydrodynamic descriptions using LMEA, LMEAC, and LFA for a dc glow discharge in argon with an applied voltage of −500 V and a pressure of 100 Pa.

for a small parameter range only [22]. Therefore, constant values for the electron mobility and diffusion coefficient have generally been used, e.g., in Ref. [28], and have been chosen in accordance with Einstein's relation [60] assuming a prescribed mean electron energy. Thus, only the rate coefficients of electron collision processes depend on the local value of $E(z,t)/N$ in the framework of common hydrodynamic models using the LFA. This procedure has also been used in the present studies.

To make direct comparisons with this method possible, in addition, calculations using rate coefficients of electron collision processes depending on the local value of $\langle U\rangle(z,t)$ as well as the same constant electron-transport properties as in the hydrodynamic description using the LFA have been performed. This approach is designated as "LMEAC."

A. Abnormal dc glow discharges

An abnormal argon glow discharge has been chosen to illustrate the influence of the different approaches for the electron properties in hydrodynamic descriptions. Figure 3 shows the particle and current densities of Ar^+ ions and electrons in steady state. The reaction kinetic model includes argon ground-state atoms, Ar^+ and Ar_2^+ ions, and electrons with their corresponding reaction channels. The utilized transport coefficients of the electrons as well as the ionization rate coefficient are presented in Figs. 10(a) and 10(b) of Appendix B. The mobility of Ar^+ and Ar_2^+ ions has been taken from Refs. [39,61], respectively, and their diffusion coefficients are determined according to the Einstein relation [60]. Furthermore, the rate coefficient for the conversion from atomic to molecular ions of 2.5×10^{-31} cm^6/s [62] and the rate coefficient for dissociative electron-molecular ion recombination given by Ref. [63], depending on the mean electron energy, have been employed.

The comparison has been performed at a discharge pressure of 100 Pa, an applied cathode voltage of −500 V, and an electrode gap of 1 cm. The coefficients of the secondary-electron emission at the cathode and of the electron reflection at the anode were chosen as 0.06 and 0.36, respectively [39]. In the description using the LFA, the transport coefficients of the electrons at the mean electron energy of 1.5 eV have been used [64]. The reflection coefficients for the positive ions were set to 5×10^{-4} [56].

The different approaches predict the same order of magnitude for the charge-carrier densities [Fig. 3(a)] as well as a qualitatively similar discharge behavior. The major differences between the results obtained by use of the LMEA and the LFA, respectively, are characterized by larger densities in the LMEA corresponding with a smaller cathode-fall thickness in comparison with the LFA. These results seem to be surprising because the rate coefficients which primarily determine the charge-carrier densities are overestimated in LFA as demonstrated in Sec. II C. But the same spatial profile of the electric field was applied for that direct comparison of the rate coefficients in LMEA and LFA.

The results presented in Fig. 3 have been obtained by means of hydrodynamic descriptions which incorporate the self-consistent determination of the space-charge field. Using the LFA, a wider cathode-fall region with a corresponding smaller electric field is predicted. Analyzing the temporal evolution of the discharge, a fundamental reason for this behavior is found in the different treatment of the electron-transport properties using either the LMEA or the LFA. In the early temporal evolution ($\sim10^{-8}$ s), the electron mobility obtained by the LMEA description decreases so that the electron propagation towards the anode is less efficient in comparison with the results using the LFA. This leads to a higher volume density of the electrons when using the LMEA causing higher ionization rates, higher space-charge densities, and therefore, a smaller cathode-fall region with higher electric field strengths. This initial difference of the electron density in the early discharge phase cannot be compensated during the rest of the temporal evolution when employing the LFA. Hence, the applied rate coefficients in the description in LFA are also smaller than the rate coefficients in LMEA resulting in the densities presented in Fig. 3(a).

The marked influence of the transport coefficients of the electrons become obvious as well from Fig. 3(a) when comparing the results of the full LMEA description with those using the LMEAC. The space-dependent electron-transport properties lead to higher absolute values of the particle densities as discussed above.

In Fig. 3(b), the corresponding current densities are presented. In particular, the cathode-fall region is well recognizable by the transition of the current dominance changing from the positive to the negative charge carriers when leaving the cathode-fall region [60]. The larger particle densities in LMEA also cause higher current densities due to the higher electric field action in a smaller spatial region in front

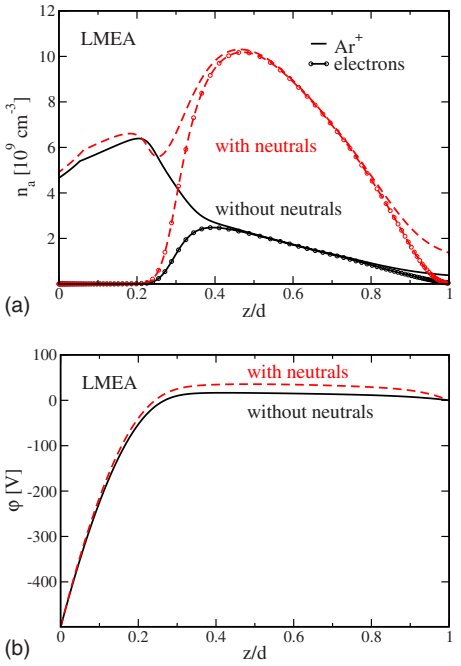

FIG. 4. (Color online) Spatial profiles of (a) the charge-carrier densities and (b) the electric potential at steady state of an abnormal argon glow discharge obtained by a hydrodynamic description using the LMEA with and without neutral species in the reaction kinetic model at an applied voltage of −500 V and a pressure of 100 Pa.

of the cathode. Using the similarity parameters of abnormal glow discharges in argon given by Engel and Steenbeck [52], the total discharge current has to be of the order of 1 to 10 $\mathrm{mA/cm^2}$. All hydrodynamic descriptions considered predict values less than the expected ones, but the LMEA results in the highest current density with about 0.5 $\mathrm{mA/cm^2}$. That means that the descriptions using the LMEA provides the best prediction for the investigated discharge.

Considering the presented discharge with a given power input instead of a given applied voltage, the general relations between all the approaches are conserved. Although the particle densities determined in LFA grow as a consequence of a required higher voltage, they are still smaller than the densities obtained by the LMEA and LMEAC. Furthermore, the thickness of the cathode-fall region in LFA remains relatively large.

The analysis presented above has been performed with a limited reaction kinetics of argon. For the improvement of the discharge description and the evaluation of the impact of excited atoms, an extended reaction kinetic model similar to that reported in Ref. [65] has been used. It takes into account several excited argon atom states including metastable, resonance, and higher excited atoms with their corresponding reaction channels.

In Fig. 4, results for the densities of electrons and Ar^+ ions as well as for the electric potential in an abnormal dc glow discharge in argon obtained by hydrodynamic descriptions using the LMEA and the extended reaction kinetic model are presented. They are compared with corresponding results neglecting the kinetics of excited states [cf. Fig. 3(a)]. It becomes obvious that the stepwise ionization processes lead to an additional charge-carrier production, resulting in higher densities of electrons and ions. In particular, both the ionization of metastable atoms and the ionization of $Ar(2p)$ atoms, mainly generated by electron-impact excitation of metastable atoms, become important because of the lower threshold energy in contrast to the direct ionization. Such behavior has also been reported by Lymberopoulos *et al.* [32] for rf discharges in argon.

The strong increase in the charge-carrier densities leads to a slight increase in the discharge current and drastically modifies the electric potential and a wide field reversal region is generated [Fig. 4(b)]. Additionally, the occurrence of a field reversal has been found to be responsible for numerical collapses of the fluid descriptions using the LFA. In agreement with Boeuf and Pitchford [34], steady-state field reversal situations have consequently not been obtained by this approach, which supposes the ionization source term as a function of the reduced electric field E/N. In general, hydrodynamic calculations using the LFA were found to be unsuitable to take into account extended reaction kinetic models.

B. Parameter variation for dc glow discharges

In the previous section, the consequences of using the LMEA and LFA in the framework of hydrodynamics descriptions have been presented for a typical argon glow discharge. A generalization of the conclusions drawn above can be done by investigations of a wide parameter range. In the present paper, the parameter pressure times gap was varied from $pd=50$ Pa cm to 1000 Pa cm and the applied voltage was considered in the range from 200 to 1000 V. The studies have been performed using the reaction kinetic model including Ar atoms, Ar^+ and Ar_2^+ ions, and electrons reported at the beginning of Sec. III A. For each set of discharge parameters, the cathode-fall thickness d_c and the cathode-fall voltage φ_c have been determined. This allows the representation of the similarity parameters pd_c and j/p^2 versus φ_c. The corresponding results for different pd are shown in Fig. 5.

Comparing the fluid modeling results obtained by use of the LMEA and LFA, respectively, with the data of Engel and Steenbeck [52], it is found that the LMEA leads to the preferred modeling results. The deviations of the LFA results from those obtained by use of the LMEA amount to more than a factor of two for pd_c [Fig. 5(a)] and to about one order of magnitude for j/p^2 [Fig. 5(b)]. In particular, results for a hydrodynamic description using the LFA for $pd=50$ Pa cm could not be obtained because an ignition of the discharge was not predicted for the range of applied voltages considered. At the same time, the increase in pd_c and the decrease in j/p^2 with decreasing cathode-fall voltage predicted by means of the LMEA at $pd=50$ Pa cm is less pronounced than for larger values of pd. This can be caused by the drift-diffusion approximation for the fluxes (12), which becomes inappropriate for too small pressures.

Furthermore, studies have been performed for oxygen glow discharges at pd between 125 and 2500 Pa cm and applied voltages from 400 to 1000 V. The reaction kinetic

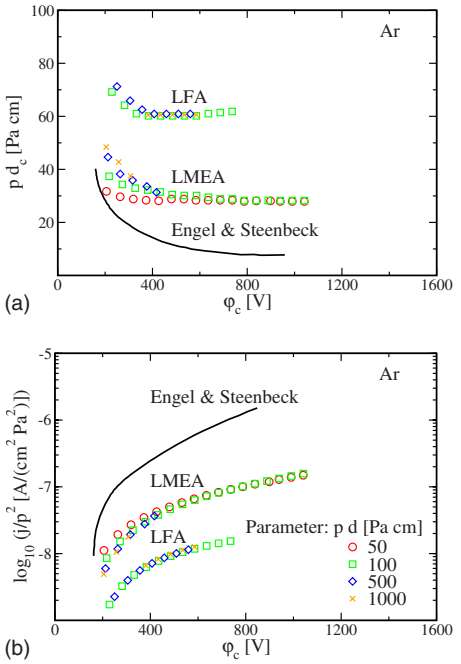

FIG. 5. (Color online) Similarity parameters (a) pd_c and (b) j/p^2 of abnormal argon glow discharges obtained by use of the LMEA and LFA in comparison with the data of Engel and Steenbeck [52].

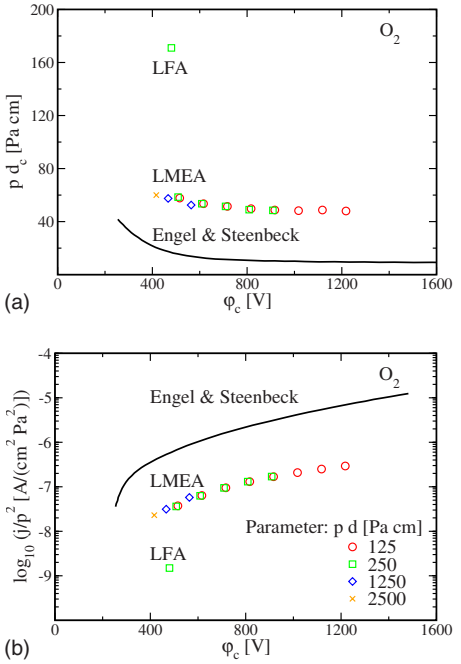

FIG. 6. (Color online) Similarity parameters (a) pd_c and (b) j/p^2 of abnormal oxygen glow discharges obtained by use of the LMEA and LFA in comparison with the data of Engel and Steenbeck [52].

model takes into account the electrons, O^- ions, and O_2^+ ions with the relevant reaction channels. In addition to the collision cross-section data used in Sec. II C, the cross section for detachment of electrons from O^- given by Refs. [66,67] and the mean electron energy-dependent rate coefficient for dissociative electron-molecular ion recombination [63] have been employed. The rate coefficients of the different collisions between heavy particles have been taken from Refs. [68,69] and the ion mobilities are reported in Ref. [70]. The secondary-electron-emission coefficient was supposed to be 0.01 and the reflection coefficients for the electrons and heavy particles have been set to the same values as for the argon discharge. The applied electron-transport coefficients and the rate coefficients for electron-impact ionization, detachment, and dissociative attachment as functions of E/N and $\langle U \rangle$ are shown in Figs. 10(c) and 10(d), respectively, of Appendix B.

Figure 6 displays the respective results for the similarity parameters pd_c and j/p^2 versus φ_c at different pd. In principle, the results obtained for oxygen discharges are very similar to those for discharges in argon. The use of the LMEA in the hydrodynamic description yields results for the entire parameter range considered, which agree qualitatively with the data reported by Engel and Steenbeck [52]. Hydrodynamic calculations employing the LFA have generally led to numerical collapse because of the reasons discussed above. The single LFA result presented in Fig. 6 again strongly overestimates the parameter pd_c and underestimates j/p^2 for a given cathode-fall voltage. This makes clear that a general application of the LFA is not possible and that the LMEA has to be preferred for the theoretical description of gas discharge plasmas.

If an extended reaction kinetic model is adapted to oxygen discharges taking neutral species such as oxygen atoms into account, the discharge behavior was found to change slightly only. The densities of neutral oxygen species remain less than 10^{-4} of the background gas density and, therefore, do not lead to drastic changes in the discharge properties.

In addition, hydrodynamic calculations using different coefficients of secondary-electron emission have been performed for the discharge parameters of the argon and oxygen discharges. Qualitative similar results have been obtained where an increase in the secondary-electron-emission coefficient leads to a better agreement for pd_c and j/p^2 in dependence on φ_c with the data of Engel and Steenbeck [52]. At the same time, the relation between the LMEA and LFA results remains almost unchanged. However, describing discharges depending on the power input instead of the applied voltage, the presented results are expected to be unchanged. Each power causes a voltage drop at the cathode that has been used in the current calculations.

C. Capacitively coupled rf discharges

The studies have additionally been extended to capacitively coupled rf discharges. Here, an application of hydrodynamic models using the LFA is not suitable because, on the one hand, the validity condition (10b) is not fulfilled and, on the other hand, Meijer *et al.* [71] have shown that the extrapolation of dc data of E/N-dependent rate coefficients to rf conditions leads to unphysical results, e.g., for the ionization rate coefficient. These conclusions could be confirmed by the authors. Applying the LFA results in density profiles for the charge carriers with a pronounced double-peak structure. In particular, these peaks of the particle densities have been found to increase continuously and to propagate to both the electrodes for a wide parameter range. This

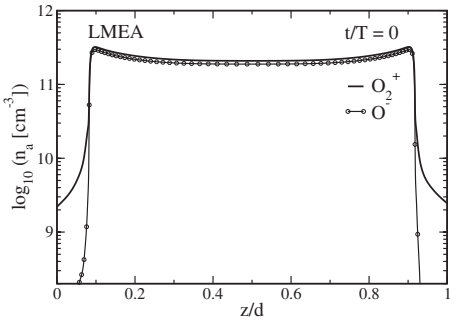

FIG. 7. Spatial profiles of the ion densities at periodic state of an rf oxygen discharge obtained by fluid descriptions using the LMEA with an applied peak-to-peak voltage of 2 kV at 100 Pa.

temporal evolution leads to steep gradients in the ion densities which finally entail a numerical collapse. Therefore, this section represents results and parameter analyses for a hydrodynamic description using the LMEA only.

In the following, an oxygen discharge at a pressure of 100 Pa, a frequency of 13.56 MHz, and an applied peak-to-peak voltage of 2 kV for an electrode gap of $d=5$ cm is considered.

The densities of the positive and negative ions at periodic state are shown in Fig. 7. The densities are almost field independent and do not vary appreciably in time. Only the values close to the boundaries change, but there is a negligible effect to the discharge volume. An almost symmetric density profile results where the particles are primarily located in the plasma bulk. This behavior is physically reasonable and coincide with experimental findings, e.g., in Ref. [72] for lower pressures. Additionally, the positively and negatively charged ion densities are of the same order of magnitude.

Figure 8 represents the corresponding density profile of the electrons at the instants $t/T=0$ and 0.25 of the period with the cycle duration T. In general, the global statements about the results are the same as for the ions presented in Fig. 7. That means, an almost symmetric density profile except for the boundary regions is found. The densities of the O_2^+ and O^- ions mainly determine the resulting space-charge density and electric potential, while the contribution of the electron density is predicted to be of minor importance.

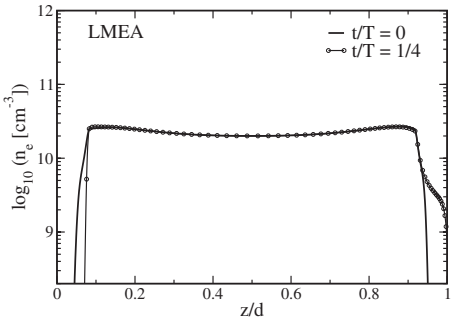

FIG. 8. Spatial profile of the electron density at periodic state of an rf oxygen discharge at $t/T=0$ and 0.25 obtained by hydrodynamic calculations using the LMEA with an applied peak-to-peak voltage of 2 kV at 100 Pa.

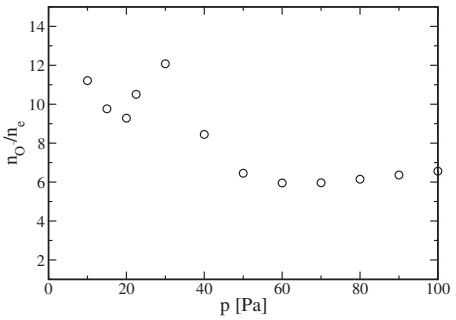

FIG. 9. Ratio of the O^- density to the electron density in the plasma bulk for rf oxygen discharges with an applied peak-to-peak voltage of 500 V at different pressures.

Elaissi *et al.* [41] have recently used a similar LMEA description to investigate the behavior of rf discharges in argon and oxygen at different discharge conditions. The direct comparison with results obtained by the present hydrodynamic model indicates, in general, good coincidence with the findings in the contribution [41], especially with respect to the shape of the ion density profiles. However, Elaissi *et al.* predicted a fast movement of a density maximum for the electron component between both the electrodes which could not be confirmed by the present investigations. Possible reasons for this difference can be attributed to different electron-transport and rate coefficients. Slightly different boundary conditions for the electrons applied by Elaissi *et al.*, which can lead to a decreased production of secondary electrons due to ion bombardment at both the electrodes, were found to be not responsible for the deviation.

D. Parameter variation for rf discharges

In order to evaluate the range of applicability of hydrodynamic descriptions using the LMEA for rf discharges, additional calculations for a wider range of discharge parameters have been performed. In particular, discharges in oxygen have been considered to determine the role of the negative ions and to compare results of the present model with available experimental data [72,73]. The studies have been done for discharges with an electrode gap of $d=5$ cm, an applied peak-to-peak voltage of 500 V, a frequency of $f=13.56$ MHz, and pressures between 10 and 100 Pa.

In Fig. 9, the ratio n_{O^-}/n_e of the density of negatively charged oxygen ions to the electron density in the plasma bulk is shown for the different discharge pressures. It can be seen that the present modeling results determine the O^- ions to be the dominant negatively charged species for the pressures considered. In particular, the density of the negative ions is one order of magnitude larger than the electron density in agreement with experimental insights reported in Ref. [73]. In addition, the magnitudes of the particle densities, e.g., $n_{O^-}=3\times10^{10}$ cm^{-3} at 25 Pa, as well as the shape of their spatial profiles, are found to be comparable with results of experimental investigations [72] as well as of recent PIC-MCC simulations [16]. Considering the power input instead of the applied voltage as calculation parameter, the presented results, in particular, Fig. 9, are almost similar. A given

power leads to a varying voltage, which can modify the absolute values of the particle densities but their ratio is not concerned.

IV. CONCLUSION

The local-mean energy approximation (LMEA) and the local-field approximation (LFA) have been analyzed and evaluated in their application for the solution of the kinetic equation of the electrons and for the self-consistent description of gas discharges by means of hydrodynamic descriptions. The studies have been performed for dc and rf discharges in argon and oxygen for a wide range of discharge parameters. The LMEA has been found to be the benchmark method for the theoretical treatment and analysis of the gas discharge plasmas on the basis of a hydrodynamic approach and it usually yields qualitative agreement when compared with a strict solution of the spatially inhomogeneous Boltzmann equation of the electrons for given reduced electric field profiles. Descriptions using the LFA cannot be recommended for the gas discharge modeling in general and their results have to be checked against experimental data or benchmark approaches.

The analysis of the plasma behavior shows, in particular, a remarkable impact of the excited species on the charge-carrier densities and potential profiles in abnormal dc glow discharges. Considering further gases like, e.g., silane or methane, similar results concerning the behavior of the LMEA and LFA are to be expected.

ACKNOWLEDGMENTS

This work was supported by the Deutsche Forschungsgemeinschaft within the SFB TR 24.

APPENDIX A: EXPANSION TECHNIQUE

Due to the investigated geometry shown in Fig. 1, the EMDF gets the reduced dependence on the coordinate z, the magnitude p of the momentum $\mathbf{p}$, and the direction cosine $p_z/p=\cos\vartheta$. Thus, the EMDF can be expanded with respect to p_z/p into Legendre polynomials $P_n(p_z/p)$. When replacing the momentum magnitude p by the kinetic energy $U=p^2/(2m_e)$, this expansion reads

$$f(z,U,\cos\vartheta,t)=2\pi(2m_e)^{3/2}\sum_{n=0}^{l-1}\tilde{f}_n(z,p,t)P_n(\cos\vartheta). \tag{A1}$$

This l-term approximation includes the isotropic part f_0 of the EMDF and all further expansion coefficients f_n with $n=1\ldots l-1$ are contributions to the anisotropy of the momentum distribution. The substitution of expansion (A1) into the kinetic equation (1) finally leads to a hierarchy of partial differential equations for the expansion coefficients $f_n(z,U,t)$ with $n=0\ldots l-1$ [4,53],

$$\begin{aligned}
0=&\sqrt{\frac{m_e}{2}}U\partial_t f_n+\frac{n}{2n-1}U\partial_z f_{n-1}+\frac{n+1}{2n+3}U\partial_z f_{n+1}\\
&+\frac{n}{2n-1}F_z^{\mathrm{ext}}\left[U\partial_U f_{n-1}-\frac{n-1}{2}f_{n-1}\right]\\
&+\frac{n+1}{2n+3}F_z^{\mathrm{ext}}\left[U\partial_U f_{n+1}+\frac{n+2}{2}f_{n+1}\right]\\
&-2\sum_a n_a\frac{m_e}{m_a}\partial_U[U^2Q_a^{\mathrm{mt}}(U)f_n]\delta_{0n}\\
&+\sum_a Un_a[Q_a^{\mathrm{mt}}(U)\theta(n-1)+\sum_i Q_{i,a}^{\mathrm{in}}(U)]f_n\\
&-\sum_a n_a\sum_i\beta_{i,a}^2(\beta_{i,a}U+U_{i,a}^{\mathrm{in}})Q_{i,a}^{\mathrm{in}}(\beta_{i,a}U+U_{i,a}^{\mathrm{in}})\\
&\times f_n(z,\beta_{i,a}U+U_{i,a}^{\mathrm{in}},t)\delta_{0n}.
\end{aligned} \tag{A2}$$

The summations in this equation take into account all individual binary collision processes of the electrons with the neutral species a, leading to elastic scattering or different kinds of inelastic collisions. On deriving system (A2), isotropic scattering of the electrons in inelastic collision processes has been assumed. Furthermore, an additional expansion of each collision integral with respect to the ratio of electron to heavy particle masses m_e/m_a has been performed. Only the leading term of each expansion has been taken into account in each hierarchy equation. The coefficient $\beta_{i,a}$ differentiates between the different kinds of inelastic electron collision processes. It is set to zero for dissociative attachment of electrons and one for excitation, dissociation, and de-excitation processes. Assuming equal energy sharing of the released binding energy between both the electrons after the ionization event, $\beta_{i,a}=2$.

When considering time-independent discharge situations and using a finite-difference representation, the resulting discrete form of the set of Eqs. (A2) is numerically solved as an initial-boundary-value problem in the space of the coordinate z and the total energy. A detailed description of the algorithm is given in Ref. [53].

APPENDIX B: ELECTRON-TRANSPORT AND RATE COEFFICIENTS

The electron mobility and diffusion coefficient for the particle (b_e,D_e) and energy $(\tilde{b}_e,\tilde{D}_e)$ transport as well as the rate coefficients of inelastic electron collisions in argon and oxygen as functions of E/N and $\langle U\rangle$, respectively, used in the present comparative studies are presented in Fig. 10. These values have been obtained by the solution of the stationary spatially homogeneous electron kinetic equation in a convergent multiterm approach using a modified version of the method presented in Ref. [45] and adapted to take nonconservative electron collision processes into account [46].

The electron properties in argon have been obtained by use of the collision cross-section data for momentum transfer in elastic scattering [74], for excitation processes in the threshold region [75], and at energies above 30 eV [74] as well as for direct ionization [76]. The drift velocity versus

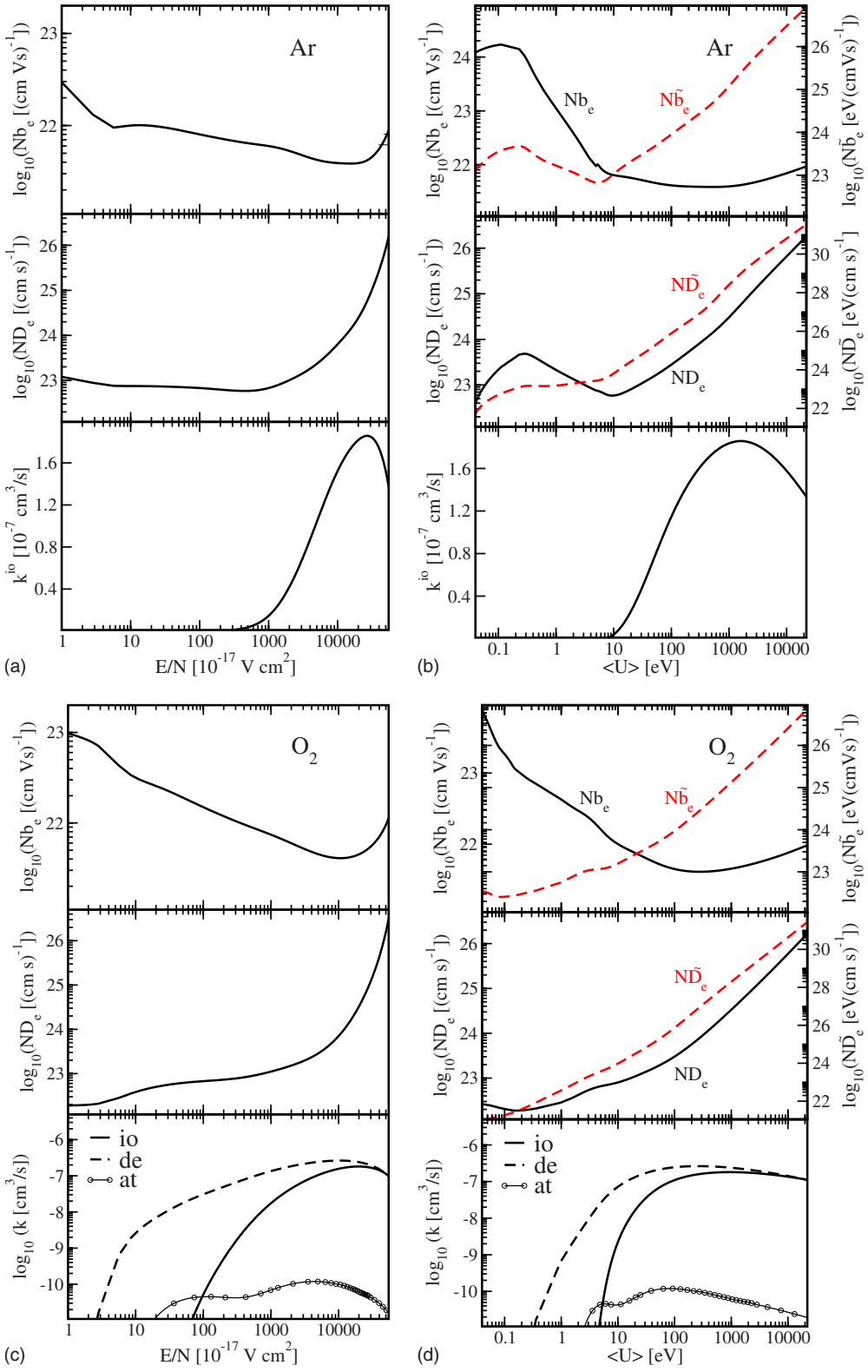

FIG. 10. (Color online) Electron transport coefficients and rate coefficient for electron-impact ionization (io), detachment (de), and attachment (at) as functions of the reduced electric field and the mean electron energy in argon and oxygen obtained by steady-state multiterm Boltzmann calculations.

the reduced electric field resulting from Fig. 10(a) shows good agreement with the experimental data of Ref. [77]. Furthermore, good agreement with the data of Ref. [78] obtained by Monte Carlo simulations has generally been found. Certain differences, e.g., for the drift velocity and mean electron energy for $E/N > 1000$ Td occur, where the present data re-

mains smaller than that of Ref. [78]. These deviations are probably due to the differences in the collisions cross sections used in the present calculations and the Monte Carlo simulations.

For oxygen discharges, the electron-impact collision cross sections for momentum transfer in elastic scattering, for vibrational excitation, dissociation, and ionization recommended by Ref. [74], the cross sections for electron-impact excitation of metastable states given by Ref. [79], and the cross section for dissociative attachment of electrons reported by Ref. [80] have been used. The drift velocity versus the reduced electric field resulting from Fig. 10(c) agrees well with the data reported in Refs. [68,81] in the range $1\ \mathrm{Td} \leq E/N \leq 1000\ \mathrm{Td}$.

There is a similar course of the electronic quantities as functions of the reduced electric field and the mean electron energy. Although the mean energy is a monotonic function of the reduced electric field, different ranges of these quantities have to be taken into account in the different modeling approaches. In particular, the whole range of E/N is used for the LFA calculations presented in this work, while the macroscopic properties as function of $\langle U \rangle$ are required for the limited range up to about 500 eV only when applying the LMEA.

[1] S. D. Rockwood, Phys. Rev. A **8**, 2348 (1973).
[2] J. Wilhelm and R. Winkler, J. Phys. Colloq. **C7**, 251 (1979).
[3] D. Loffhagen and R. Winkler, J. Phys. D **29**, 618 (1996).
[4] G. Petrov and R. Winkler, J. Phys. D **30**, 53 (1997).
[5] H. Sugawara, Y. Sakai, H. Tagashira, and K. Kitamori, J. Phys. D **31**, 319 (1998).
[6] R. E. Robson, P. Nicoletopoulos, B. Li, and R. D. White, Plasma Sources Sci. Technol. **17**, 024020 (2008).
[7] J. P. Boeuf and E. Marode, J. Phys. D **15**, 2169 (1982).
[8] Z. Donkó, K. Rózsa, and R. C. Tobin, J. Phys. D **29**, 105 (1996).
[9] D. Loffhagen, F. Sigeneger, and R. Winkler, Eur. Phys. J.: Appl. Phys. **25**, 45 (2004).
[10] S. Longo, Plasma Sources Sci. Technol. **15**, S181 (2006).
[11] S. Dujko, R. D. White, and Z. L. Petrovic, J. Phys. D **41**, 245205 (2008).
[12] R. W. Boswell and I. J. Morey, Appl. Phys. Lett. **52**, 21 (1988).
[13] C. Birdsall, IEEE Trans. Plasma Sci. **19**, 65 (1991).
[14] V. Vahedi, C. Birdsall, M. Lieberman, G. DiPeso, and T. Rognlien, Plasma Sources Sci. Technol. **2**, 273 (1993).
[15] M. M. Turner, Phys. Plasmas **13**, 033506 (2006).
[16] F. X. Bronold, K. Matyash, D. Tskhakaya, R. Schneider, and H. Fehske, J. Phys. D **40**, 6583 (2007).
[17] S. Pfau and R. Winkler, Beitr. Plasmaphys. **20**, 343 (1980).
[18] M. J. Kushner, J. Appl. Phys. **63**, 2532 (1988).
[19] J. P. Boeuf and L. Pitchford, IEEE Trans. Plasma Sci. **19**, 286 (1991).
[20] A. Bogaerts, R. Gijbels, and W. J. Goedheer, J. Appl. Phys. **78**, 2233 (1995).
[21] Z. Donkó, Phys. Rev. E **57**, 7126 (1998).
[22] Z. Donkó, P. Hartmann, and K. Kutasi, Plasma Sources Sci. Technol. **15**, 178 (2006).
[23] F. Sigeneger, Z. Donkó, and D. Loffhagen, Eur. Phys. J.: Appl. Phys. **38**, 161 (2007).
[24] D. Loffhagen and F. Sigeneger, Plasma Sources Sci. Technol. **18**, 034006 (2009).
[25] A. L. Ward, J. Appl. Phys. **33**, 2789 (1962).
[26] P. Bayle, J. Vacquie, and M. Bayle, Phys. Rev. A **34**, 360 (1986).
[27] D. Graves and K. F. Jensen, IEEE Trans. Plasma Sci. **14**, 78 (1986).
[28] J. P. Boeuf, Phys. Rev. A **36**, 2782 (1987).
[29] A. D. Richards, B. E. Thompson, and H. H. Sawin, Appl. Phys. Lett. **50**, 492 (1987).
[30] S. K. Park and D. J. Economou, J. Appl. Phys. **68**, 3904 (1990).
[31] M. Meyyappan and J. P. Kreskovsky, J. Appl. Phys. **68**, 1506 (1990).
[32] D. P. Lymberopoulos and D. J. Economou, J. Appl. Phys. **73**, 3668 (1993).
[33] H. Akashi, Y. Sakai, and T. Tagashira, J. Phys. D **27**, 1097 (1994).
[34] J. P. Boeuf and L. Pitchford, J. Phys. D **28**, 2083 (1995).
[35] J. P. Boeuf and L. C. Pitchford, Phys. Rev. E **51**, 1376 (1995).
[36] J. H. Ingold, Phys. Rev. E **56**, 5932 (1997).
[37] L. C. Pitchford, I. Peres, K. B. Liland, J. P. Boeuf, and H. Gielen, J. Appl. Phys. **82**, 112 (1997).
[38] G. Steinle, D. Neundorf, W. Hiller, and M. Pietralla, J. Phys. D **32**, 1350 (1999).
[39] A. V. Phelps and Z. L. Petrovic, Plasma Sources Sci. Technol. **8**, R21 (1999).
[40] A. Phelps, Plasma Sources Sci. Technol. **10**, 329 (2001).
[41] S. Elaissi, M. Yousfi, H. Helali, S. Kazziz, K. Charrada, and M. Sassi, Plasma Devices Oper. **14**, 27 (2006).
[42] I. A. Porokhova, J. Winter, F. Sigeneger, D. Loffhagen, and H. Lange, Plasma Sources Sci. Technol. **18**, 015013 (2009).
[43] G. G. Lister, J. Phys. D **25**, 1649 (1992).
[44] J. Wilhelm and R. Winkler, Ann. Phys. **23**, 28 (1969).
[45] H. Leyh, D. Loffhagen, and R. Winkler, Comput. Phys. Commun. **113**, 33 (1998).
[46] N. R. Pinhao, Z. Donkó, D. Loffhagen, M. J. Pinheiro, and E. A. Richley, Plasma Sources Sci. Technol. **13**, 719 (2004).
[47] G. J. M. Hagelaar and L. C. Pitchford, Plasma Sources Sci. Technol. **14**, 722 (2005).
[48] F. Sigeneger and R. Winkler, IEEE Trans. Plasma Sci. **27**, 1254 (1999).
[49] R. Winkler, D. Loffhagen, and F. Sigeneger, Appl. Surf. Sci. **192**, 50 (2002).
[50] G. Simon and W. Bötticher, J. Appl. Phys. **76**, 5036 (1994).
[51] P. L. Morton, Phys. Rev. **70**, 358 (1946).
[52] A. Engel and M. Steenbeck, *Elektrische Gasentladungen—ihre Physik und Technik* (Springer, Berlin, 1934).
[53] G. K. Grubert and D. Loffhagen, IEEE Trans. Plasma Sci. **35**, 1215 (2007).
[54] S. Arndt, F. Sigeneger, and R. Winkler, Plasma Chem. Plasma

Process. **23**, 439 (2003).
[55] R. Winkler and M. W. Wuttke, Appl. Phys. B: Lasers Opt. **54**, 1 (1992).
[56] V. E. Golant, A. P. Zhilinsky, and I. E. Sakharov, *Fundamentals of Plasma Physics* (Wiley, New York, 1980).
[57] M. M. Becker, D. Loffhagen, and W. Schmidt, Comput. Phys. Commun. **180**, 1230 (2009).
[58] G. Hagelaar and G. Kroesen, J. Comput. Phys. **159**, 1 (2000).
[59] G. J. M. Hagelaar, F. J. de Hoog, and G. M. W. Kroesen, Phys. Rev. E **62**, 1452 (2000).
[60] Y. P. Raizer, *Gas Discharge Physics* (Springer, Berlin, 1991).
[61] H. W. Ellis, M. G. Thackston, and E. W. McDaniel, At. Data Nucl. Data Tables **31**, 113 (1984).
[62] E. W. McDaniel, V. Čermak, A. Dalgarno, E. E. Fergusson, and L. Friedman, *Ion-Molecule Reactions* (Wiley-Interscience, New York, 1970).
[63] J. N. Bardsley and M. A. Biondi, *Dissociative Recombination* (Academic Press, New York, 1970), Vol. 6, pp. 1–57.
[64] K. Kutasi and Z. Donkó, J. Phys. D **33**, 1081 (2000).
[65] S. Gorchakov, D. Loffhagen, and D. Uhrlandt, Phys. Rev. E **74**, 066401 (2006).
[66] B. Peart, R. Forrest, and K. T. Dolder, J. Phys. B **12**, 847 (1979).
[67] B. Peart, R. Forrest, and K. Dolder, J. Phys. B **12**, 2735 (1979).
[68] B. Eliasson and U. Kogelschatz, Brown Boveri Forschungszentrum Report No. KLR 86–11 C, 1986, (unpublished).
[69] J. A. Wagner and H. M. Katsch, Plasma Sources Sci. Technol. **15**, 156 (2006).
[70] H. W. Ellis, R. Y. Pai, E. W. McDaniel, E. A. Mason, and L. A. Viehland, At. Data Nucl. Data Tables **17**, 177 (1976).
[71] P. M. Meijer, W. J. Goedheer, and J. D. P. Passchier, Phys. Rev. A **45**, 1098 (1992).
[72] H. M. Katsch, T. Sturm, E. Quandt, and H. F. Döbele, Plasma Sources Sci. Technol. **9**, 323 (2000).
[73] E. Stoffels, W. W. Stoffels, D. Vender, M. Kando, G. M. W. Kroesen, and F. J. de Hoog, Phys. Rev. E **51**, 2425 (1995).
[74] M. Hayashi, *Electron Collision Cross Sections* (Ohmsha Ltd., Tokyo, 1992), pp. 748–766.
[75] O. Zatsarinny and K. Bartschat, J. Phys. B **37**, 4693 (2004).
[76] D. Rapp and P. Englander-Golden, J. Chem. Phys. **43**, 1464 (1965).
[77] Y. Nakamura and M. Kurachi, J. Phys. D **21**, 718 (1988).
[78] S. Kondo and K. Nanbu, Rep. Inst. Fluid Sci., Tohoku Univ. **12**, 101 (2000).
[79] K. Wakiya, J. Phys. B **11**, 3913 (1978).
[80] D. Rapp and D. Briglia, J. Chem. Phys. **43**, 1480 (1965).
[81] J. Dutton, J. Phys. Chem. Ref. Data **4**, 577 (1975).